All-Optical Switching in *Pharaonis* Phoborhodopsin Protein Molecules

Sukhdev Roy*, Takashi Kikukawa, Parag Sharma, *Student Member, IEEE*, and Naoki Kamo

***Abstract*—Low-power all-optical switching with *pharaonis* phoborhodopsin (*p*pR) protein is demonstrated based on nonlinear excited-state absorption at different wavelengths. A modulating pulsed 532-nm laser beam is shown to switch the transmission of a continuous-wave signal light beam at: 1) 390 nm; 2) 500 nm; 3) 560 nm; and 4) 600 nm, respectively. Simulations based on the rate equation approach considering all seven states in the *p*pR photocycle are in good agreement with experimental results. It is shown that the switching characteristics at 560 and 600 nm, respectively, can exhibit negative to positive switching. The switching characteristics at 500 nm can be inverted by increasing the signal beam intensity. The profile of switched signal beam is also sensitive to the modulating pulse frequency and signal beam intensity and wavelength. The switching characteristics are also shown to be sensitive to the lifetimes of $p\mathrm{pR_M}$ and $p\mathrm{pR_O}$ intermediates. The results show the applicability of *p*pR as a low-power wavelength tunable all-optical switch.**

***Index Terms*—Bacteriorhodopsin, optical modulation, optical switching.**

I. Introduction

RECENT developments in nanophotonics have given impetus to synthesize novel photosensitive molecules for all-optical information processing [1], [2]. The possibility of tailoring the nonlinear optical response at the molecular level coupled with advantages of small size and weight, low propagation delay, and power dissipation make interesting prospects for optimized device applications [1], [2].

The naturally occurring photosensitive biological molecules optimized over centuries of evolution offer exciting possibilities for device applications. The photochromic bacteriorhodopsin (bR) protein found in the purple membrane of *Halobacterium halobium* has by far received the most attention for a wide range of biomolecular photonic applications [3]–[7].

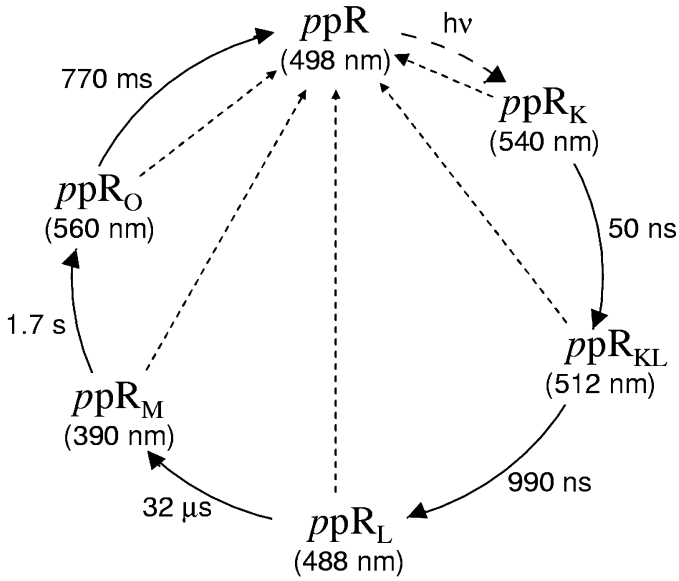

Fig. 1. Schematic of the typical photocycle of *p*pR molecule. The maximum absorption wavelengths of the intermediates are shown in brackets. Solid and dashed arrows represent thermal and photoinduced transitions, respectively.

A switch is the basic building block of information processing systems. Recently, there has been considerable research interest in using the photochromic properties of bR to design an all-optical switch [8]–[16]. All-optical switching in bacteriorhodopsin has been reported using multiple-laser geometries involving holograms [8], [9], refractive index modulation [10], enhanced photoinduced anisotropy, and excited-state absorption [11]–[16]. Most of these studies are based on the pump-probe technique in which a continuous-wave (cw) probe beam is switched by a pulsed pump beam. Our analysis of all-optical light modulation in bR shows that longer lifetimes of the intermediate states lead to low-power operation [13], [14].

Recently, a new photoreceptor sensory rhodopsin II (sRII) or phoborhodopsin (pR) like protein, synthesized from *Natronobacterium pharaonis*, a halophilic alkaliphilic bacterium termed *pharaonis* phoborhodopsin (*p*pR), has received much attention due to its good stability and recent structure elucidation [17]–[21]. Among the archaeal sensory rhodopsins, *p*pR has the most robust properties and is able to function during photosignaling in *N. pharaonis*, *H. salinarium*, and *Escherichia coli*. *Np*SRII or *p*pR remains stable both in the dark and under prolonged illumination, and it retains its native absorption spectrum and photocycle in different membranes; in a range of detergents; in salt concentrations from 25 to 4 M; and

Manuscript received November 18, 2005; revised May 22, 2006. This work was supported in part by the Department of Science and Technology, Government of India, under Grant SP/S2/L-07/2000. The work of S. Roy was supported by a Career Award for Young Teachers by the All India Council for Technical Education under Grant FD/CA(05)/2001–2002 and the Japan Society for Promotion of Science Invitation Fellowship, under which the experiments were performed. The work of P. Sharma was supported by the Senior Research Fellowship from the Council of Scientific and Industrial Research, India. *Asterisk indicates corresponding author.*

*S. Roy is with the Department of Physics and Computer Science, Dayalbagh Educational Institute (Deemed University), Agra 282 005, India (e-mail: sukhdevr@hotmail.com).

P. Sharma is with the Department of Physics and Computer Science, Dayalbagh Educational Institute (Deemed University), Agra 282 005, India (e-mail: paragsharma22@rediffmail.com).

T. Kikukawa is with the Creative Research Initiative "Sosei" (CRIS), Hokkaido University, Sapporo 001 0021, Japan (e-mail: kikukawa@cast.hokudai.ac.jp).

N. Kamo is with the Laboratory of Biophysical Chemistry, Graduate School of Pharmaceutical Sciences, Hokkaido University, Sapporo 060-0812, Japan (e-mail: nkamo@pharm.hokudai.ac.jp).

Digital Object Identifier 10.1109/TNB.2006.880828

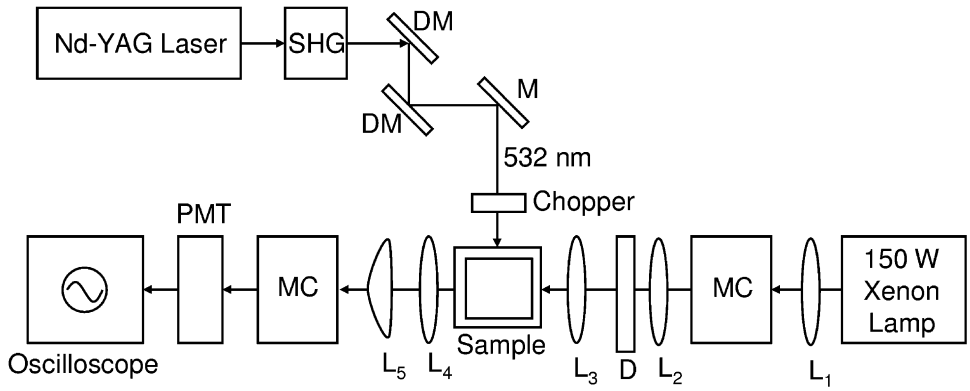

Fig. 2. Experimental setup for all-optical switching in *p*pR. DM: dichroic mirror. M: mirror. MC: monochromator. L: lens. D: depolarizer.

over a broad range of pH. These exceptional properties have made it the prototypical sensory rhodopsin for crystallography and structure/function studies [17]. It exhibits a blue-shifted photocycle similar to bR as shown in Fig. 1 [21]. After excitation with 498-nm wavelength light, the molecule gets excited from the initial *p*pR state to the $p\text{pR}_K$ state and transforms to the $p\text{pR}_{\text{KL}}$ state within 50 ns. From there it transforms in 990 ns into the $p\text{pR}_L$ state. From the $p\text{pR}_L$ state, the molecules transform to the $p\text{pR}_M$ state in about 32 μs. The species in the $p\text{pR}_M$ state relax to the $p\text{pR}_O$ intermediate state in 1.7 s, from which it finally relaxes to the initial *p*pR state in 770 ms. The intermediates are named in analogy to those in the photocycle of bR.

The *p*pR photocycle exhibits longer lifetimes of the $p\text{pR}_M$ and the $p\text{pR}_O$ intermediate states even in its native state, i.e., the wild-type (WT) form, and hence leads to all-optical light modulation at considerably lower modulating pump powers in comparison to bR. Recently, we have reported theoretical designs of low-power all-optical spatial light modulators and logic gates with WT-*p*pR and its mutants [22]–[24].

For all-optical information processing, it is important to have the capability to effectively control the switching characteristics. Moreover, for digital operation, it is necessary to perform all-optical switching with a train of modulating pulses. All-optical switching based on the principle of excited-state absorption, using a pump-probe configuration, is a simple, flexible, and convenient technique for practical applications, compared to other methods, for instance, those based on phase conjugation and interference phenomena. The switching characteristics using the pump-probe configuration, with pulse train excitation, would be similar to the single modulating pulse excitation, provided the period of the modulating pulse train is greater than the switching time of the switched signal beam due to single modulating pulse excitation. An increase in modulating pulse frequency would affect the nature and contrast of switching characteristics. Thus, it is important to study the effect of the modulating pulse frequency on the switching characteristics. In addition to this, the existence of different intermediates that exhibit respective absorption spectra spanning the entire visible range, provides interesting opportunity to switch the transmission of probe (signal) beams at different wavelengths. Hence, it would be interesting to investigate the all-optical control of: 1) the switching characteristics to realize positive or negative switching and 2) the switched signal beam pulse profile that have not been reported as yet.

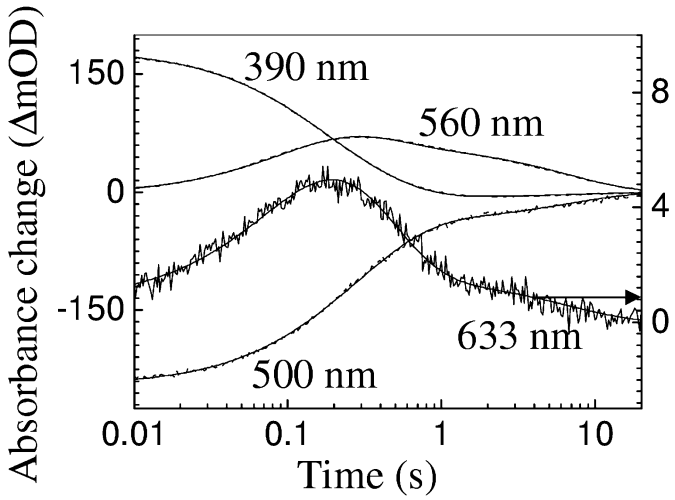

Fig. 3. Flash-photolysis kinetic data at 390, 500, 560, and 633 nm for WT-*p*pR with imidazole.

The aim of this paper is to experimentally investigate: 1) all-optical switching in this new *p*pR protein based on excited-state absorption; 2) the effect of modulating pulse frequency; 3) the effect of signal beam wavelength at 390, 500, and 560 nm, which correspond to the peak absorption of the $p\text{pR}_M$, *p*pR, and $p\text{pR}_O$ states, respectively, and also at 600 nm; 4) the effect of modulating beam and signal beam intensity, on the apparent phase shifting of the switched signal beam with respect to pulsed modulating beam; and 5) to explain the experimental results theoretically. We demonstrate a simple, mirrorless all-optical switch with *p*pR. We show that the switching characteristics, i.e., the apparent shifting of the switched signal beam with respect to modulating pulses and the profile of the switched pulses, are sensitive to the modulating pulse frequency, signal beam intensity, and wavelength. Theoretical simulations using the rate equation approach are in good agreement with experimental results.

II. Experimental Setup and Material Characterization

The WT-*p*pR sample was prepared by following the procedure reported earlier [20]. The concentration of *p*pR in the sample was 53 μM. Fig. 2 shows the experimental setup. A vertically polarized second harmonic of Nd-YAG laser beam

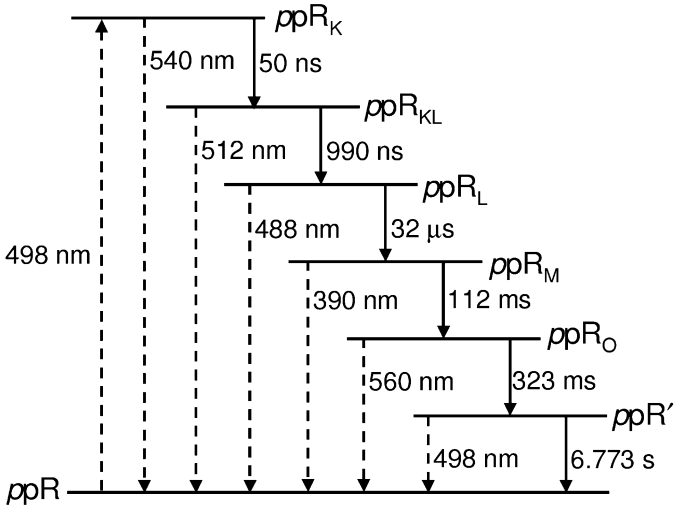

Fig. 4. Simplified level diagram representing the photocycle of *p*pR sample. Solid and dashed arrows have the same meaning as in Fig. 1.

(532 nm) at 5 mW of 5 mm diameter was used as the modulating beam. Signal light beams at different wavelengths, respectively, were taken from a monochromator which was illuminated by a 150-W Xenon lamp. The depolarized signal beam had a diameter of 3 mm. The modulating beam overlapped with the signal beam over a 5-mm length in the sample placed in a quartz cuvette. To select the measuring signal wavelength and exclude the scattered modulating light from the sample, another monochromator was placed in front of the photomultiplier tube (PMT). The output of the PMT was connected to a digital storage oscilloscope.

The *p*pR sample was characterized using computer-controlled flash photolysis [20]. Interestingly, an additional *p*pR′ intermediate state after the $p\mathrm{pR}_O$ state, having absorption spectrum similar to the initial *p*pR state, was observed, due to three exponential global fitting for the absorbance changes at 390-, 500-, and 560-nm wavelengths, as shown in Fig. 3. The lifetimes of the three long lifetime $p\mathrm{pR}_M$, $p\mathrm{pR}_O$ and *p*pR′ intermediate states in the photocycle, were measured to be 112 ms, 323 ms, and 6.773 s, respectively, which are considerably lower than typical values due to the presence of imidazole, which accelerates the decay of $p\mathrm{pR}_M$ and $p\mathrm{pR}_O$ intermediates.

III. Theoretical Model

We introduce a simplified level diagram shown in Fig. 4 to represent the photocycle of *p*pR molecules of the sample, which enables the adoption of the simple rate equation approach for the population densities in the various intermediates. To simulate the effect of the intensities of both the modulating and signal beams, we consider the *p*pR molecules exposed to light beams of intensities I'_m and I'_s, which modulate the population densities of different intermediate states through the excitation and de-excitation processes. These can be described by the rate equations in the following form [14], [22]–[24]:

$$\begin{aligned}\frac{dN_1(t)}{dt} &= -(I_m\sigma_1\psi + I_s\sigma_{1s})N_1(t) \\ &\quad + \sum_{i=2}^{7}(I_m\sigma_i + I_s\sigma_{is})N_i(t) + k_7N_7(t) \\ \frac{dN_2(t)}{dt} &= (I_m\sigma_1\psi + I_s\sigma_{1s})N_1(t) \\ &\quad - (k_2 + I_m\sigma_2 + I_s\sigma_{2s})N_2(t) \\ \frac{dN_j(t)}{dt} &= k_{j-1}N_{j-1}(t) - (k_j + I_m\sigma_j + I_s\sigma_{js})N_j(t) \\ &\quad \text{for } j = 3 \text{ to } 7 \end{aligned} \tag{1}$$

where N_i, $i = 1$ to 7 represents the population densities of *p*pR, $p\mathrm{pR}_K$, $p\mathrm{pR}_{\mathrm{KL}}$, $p\mathrm{pR}_L$, $p\mathrm{pR}_M$, $p\mathrm{pR}_O$, and *p*pR′ states, respectively; σ_i and k_i are the absorption cross sections and rate constants of respective states; subscript s denotes the value at signal wavelength; and $\psi = 0.51$ is the quantum efficiency for the $p\mathrm{pR} \rightarrow p\mathrm{pR}_K$ transition [19]. I_m and I_s are the photon density fluxes of the modulating laser and signal beams, respectively, i.e., ratio of the intensity to the photon energy $h\nu$ at respective wavelengths.

The modulating laser beam pulses are considered to have a super-Gaussian pulse profile given by

$$I'_m = I'_{m0}\exp\left(-c\left(\frac{t - t_m}{\Delta t}\right)^{2q}\right) \tag{2}$$

where t_m is the time at which the respective pulse maxima occur, $c = 2^{2q}ln\ 2$ is the pulse profile parameter and Δt is the pulsewidth and q is an integer, which determines the shape of the pulse [14].

We consider the transmission of a cw signal light beam of intensity I'_s modulated by absorption due to different intermediate states that get populated due to excitation of *p*pR molecules by both the pulsed modulating laser and signal beams. The nonlinear intensity-dependent absorption coefficient for the signal beam is written as

$$\alpha_s(I_m, I_s) = \sum_{i=1}^{7} N_i(I_m, I_s)\sigma_{is} \tag{3}$$

where the subscript s denotes the value at signal wavelength. The propagation of the signal beam through the *p*pR sample is governed by

$$\frac{dI_s}{dx} = -\alpha_s(I_m, I_s)I_s. \tag{4}$$

The normalized transmitted signal intensity (TSI) can be written as

$$\frac{I_{\mathrm{sout}}}{I_{\mathrm{sin}}} = \exp\{-\alpha_s(I_m, I_s)L\} \tag{5}$$

where L is the thickness of the sample.

IV. Results and Discussion

The all-optical switching characteristics of the *p*pR sample were studied for different signal beam wavelengths (390, 500, 560, and 600 nm), for modulating pulses at 532 nm, over a wide range of modulating pulse frequencies (0.05–20 Hz). Fig. 5 shows the experimental curves for $p\mathrm{pR}_O$ state dynamics, i.e., variation of TSI at 560 nm that corresponds to peak absorption

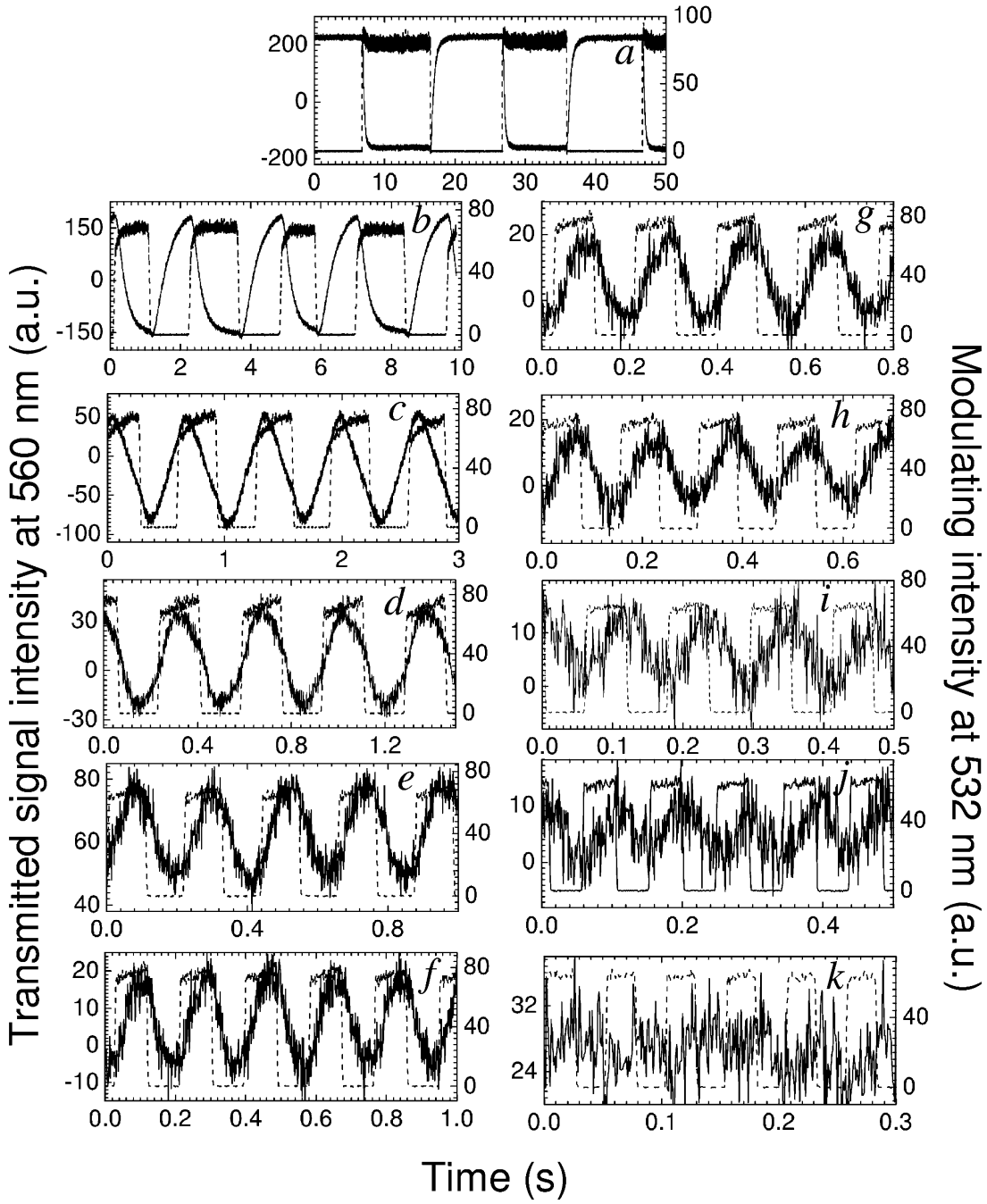

Fig. 5. Measured TSI at 560 nm (solid lines) and input modulating beam at 532 nm (dashed lines) for modulating pulse frequency: (a) 0.05 Hz; (b) 0.42 Hz; (c) 1.53 Hz; (d) 2.86 Hz; (e) 5 Hz; (f) 5.42 Hz; (g) 6.42 Hz; (h) 6.86 Hz; (i) 8.57 Hz; (j) 10.55 Hz; and (k) 19.52 Hz.

of $p\text{pR}_O$ intermediate state, switched by a modulating pulse train at 532 nm, for different modulating pulse frequencies. The switched signal beam exhibits out-of-phase characteristics with respect to modulating pulse (negative switching), for single pulse excitation or for a pulse train at low frequencies as shown in Fig. 5(a). Initially, in the absence of the modulating pulse, all protein molecules stay in the initial *p*pR state, hence, the TSI is high (ON state) due to less linear absorption of signal beam by initial *p*pR state only. As the modulating pulse excites the *p*pR molecules, the population of longer lived $p\text{pR}_O$ intermediate increases, which leads to increased absorption of the signal beam and hence switching OFF of the TSI. This results in the basic all-optical switching mechanism, as shown in Fig. 5(a).

Increase in modulating pulse frequency to larger values results in an apparent phase shift of TSI with respect to the modulating pulse as shown in Fig. 5(d)–(k). For a modulating pulse train, the presence of a second successive pulse at a time interval less than the relaxation time of the photocycle, results in the TSI not reaching the steady-state OFF-ON values. This results in a decrease in contrast and an asymmetric switched signal profile, while maintaining out-of-phase switching behavior, as is evident from Fig. 5(b). Increasing the frequency further results in a symmetric triangular profile, Fig. 5(c). This apparent phase shift of TSI saturates after a certain value, maintaining the switched signal profile and exhibits a continuous decrease in contrast.

TABLE I
ABSORPTION CROSS SECTIONS AND RATE CONSTANTS OF DIFFERENT INTERMEDIATES OF PPR [20]–[24]

Rate Constant	WT-*p*pR Value(s^{-1})	Absorption Cross-Section	Value (cm^2)				
			532 nm	390 nm	500 nm	560 nm	600 nm
		σ_1	5.60×10^{-17}	3.2×10^{-17}	1.6×10^{-16}	1.6×10^{-17}	Ö
k_2	2.0×10^7	σ_2	Ö	Ö	6.4×10^{-17}	Ö	Ö
k_3	1.0×10^6	σ_3	1.08×10^{-16}	3.2×10^{-17}	1.3×10^{-16}	4.3×10^{-17}	Ö
k_4	3.1×10^4	σ_4	4.64×10^{-17}	3.2×10^{-17}	1.0×10^{-16}	1.6×10^{-17}	Ö
k_5	8.93	σ_5	1.30×10^{-16}	1.5×10^{-16}	Ö	Ö	Ö
k_6	3.09	σ_6	Ö	3.2×10^{-17}	4.4×10^{-17}	1.76×10^{-16}	6.77×10^{-17}
k_7	0.148	σ_7	5.60×10^{-17}	3.2×10^{-17}	1.6×10^{-16}	1.6×10^{-17}	Ö

As the modulating pulse appears, the TSI switches off after a certain time lag. This time lag appears due to the time taken by the molecules to relax from the long lifetime $p\mathrm{pR}_M$ intermediate that does not absorb the signal beam at 560 nm, to the probed $p\mathrm{pR}_O$ state. This time lag appears to be significant at higher modulating pulse frequencies, when it becomes comparable to the modulating pulse width, which is evident from Fig. 5(d)–(k).

Theoretical simulations have been carried out by numerically solving the nonlinear time-dependent equations (1)–(5), using the experimentally measured lifetimes of the $p\mathrm{pR}_M$, $p\mathrm{pR}_O$, and $p\mathrm{pR}'$ states and the typical values of other parameters reported in literature as given in Table I [20]–[24].

Fig. 6 shows the corresponding theoretically simulated optical switching curves for $p\mathrm{pR}_O$ state dynamics, considering the experimental conditions and pulse profile parameter $q = 8$. It is evident from Figs. 5 and 6 that simulated results are in good accord with experimental results. The theoretical results are in good agreement at relatively lower intensity values. This may be attributed to the effective absorption after considering reflection and scattering losses.

To study the switching characteristics at different wavelengths, we carried out experiments with signal beams at 390, 500, and 600 nm also that correspond to the peak absorption wavelengths of $p\mathrm{pR}_M$, *p*pR, and near the peak absorption wavelength of $p\mathrm{pR}_O$ state, respectively. The experimental results are shown in Fig. 7(a)–(d) at modulating pulse frequency of 5 Hz.

Fig. 7(a) shows the variation of TSI at 390 nm corresponding to the peak absorption of $p\mathrm{pR}_M$ intermediate state with time. For single modulating pulse excitation, initially, in the absence of the modulating pulse, the linear TSI at 390 nm is high due to small absorption by initial *p*pR state only [21]. As the modulating pulse appears, the TSI at 390 nm decreases from its linear value due to absorption by the longer lived $p\mathrm{pR}_M$ state, exhibiting out-of-phase characteristics (negative switching) with respect to modulating pulse.

As shown in Fig. 7(a), for modulating pulse train at high frequency (5 Hz), the TSI at 390 nm also shows negative switching and does not show any apparent phase shift with respect to modulating pulses due to very small time ($\sim \mu$s) taken by $p\mathrm{pR}_L$ state molecules to relax to $p\mathrm{pR}_M$ intermediate probed state.

Fig. 7(b) shows the variation of TSI at 500 nm, corresponding to the peak absorption of initial *p*pR state with time. For, single modulating pulse excitation, the linear TSI at 500 nm is low due to its high absorption by initial *p*pR state [20], [21]. As the modulating pulse excites the molecules, the TSI at 500 nm increases due to decrease in the population of initial *p*pR state. The TSI saturates to its initial value after the passage of the modulating pulse due to relaxation of excited molecules back to the initial state. Thus, the TSI at 500 nm shows positive switching for broad modulating pulses at lower frequencies and also at 5 Hz modulating pulse frequency as shown in Fig. 7(b).

The variation of TSI at 560 nm, corresponding to the peak absorption of $p\mathrm{pR}_O$ intermediate state with time, is shown in Fig. 7(c), for comparison. The switching characteristics are inverted (positive switching) in comparison to low modulating pulse frequency case [negative switching, Fig. 5(a)], due to apparent phase shift as described earlier.

Fig. 7(d) shows the variation of TSI at 600 nm with time. The switching characteristics in this case also are inverted (positive switching) in comparison to negative switching exhibited at low modulating pulse frequencies. This is due to $p\mathrm{pR}_O$ state dynamics, as the signal wavelength is nearer to the peak absorption wavelength of $p\mathrm{pR}_O$ intermediate (560 nm).

The corresponding theoretically simulated optical switching curves for different signal beam wavelengths, considering the experimental conditions, for pulse profile parameter $q = 10$ are shown in Fig. 8. It is evident from Figs. 7 and 8 that simulated results agree well with experimental results.

Thus, the apparent phase shift of TSI with respect to modulating pulses is sensitive to the signal beam wavelength and frequency f. Our theoretical simulations show that it can be continuously varied between some specific ranges at different signal beam wavelengths, for a given frequency range.

It is also evident from Figs. 7 and 8 that the profile of the switched TSI is sensitive to the wavelength of the signal beam. For instance, the TSI at 390 and 500 nm has triangular profile, whereas it is like a sinusoid at 560 and 600 nm. The profile of the switched TSI is also sensitive to frequency. For broad pulses, TSI attains steady-state off–on values, and exhibits symmetric

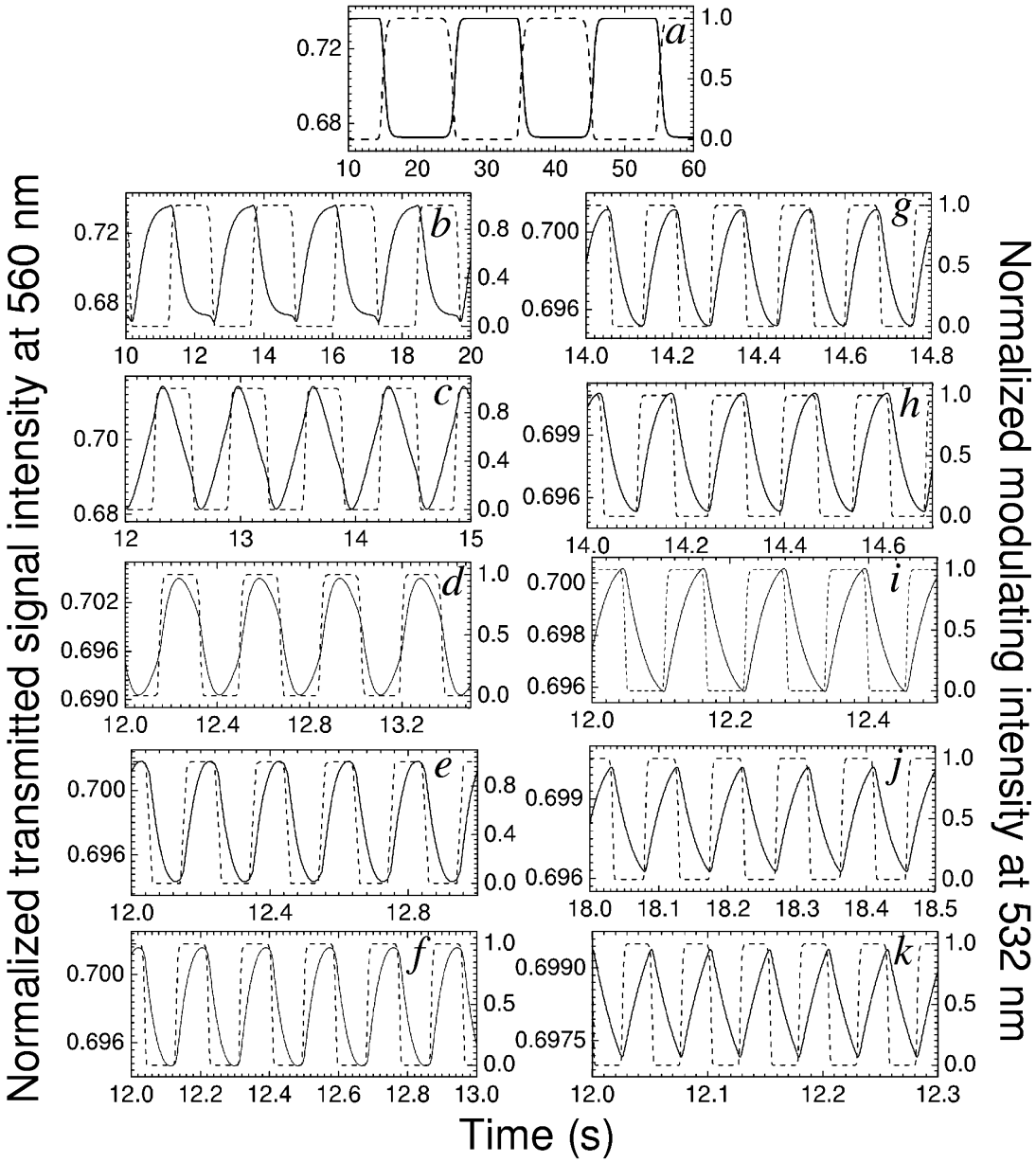

Fig. 6. Simulated normalized TSI at 560 nm (solid lines), and input modulating beam at 532 nm (dashed lines) for modulating pulse frequency: (a) 0.05 Hz; (b) 0.42 Hz; (c) 1.53 Hz; (d) 2.86 Hz; (e) 5 Hz; (f) 5.42 Hz; (g) 6.42 Hz; (h) 6.86 Hz; (i) 8.57 Hz; (j) 10.55 Hz; and (k) 19.52 Hz, for peak modulating power of 1 mW and signal beam of 0.2 mW.

profile. On increase in frequency, the TSI is unable to reach the steady state, as the molecules are unable to relax to the initial or probed excited state, which results in lower contrast and an asymmetric profile that becomes symmetric at higher values.

Theoretical simulations for $p\mathrm{pR}_O$ state dynamics show that the switching contrast $(\mathrm{TSI}_{\max} - \mathrm{TSI}_{\min})$ decreases exponentially after a certain frequency value, whereas, apparent phase shift varies monotonically with frequency, in the range $0.05 \leq f \leq 5$ Hz, Fig. 6. The switch OFF and ON times are 1.3 and 1.1 s for $f = 0.42$ Hz; and 59 and 58 ms for $f = 8.57$ Hz, respectively. The switching contrast can be increased by using the modulating beam at 498 nm, which is the peak absorption wavelength of initial *p*pR state.

The apparent phase shift is also sensitive to the kinetic parameters of *p*pR photocycle. The rate constants of the intermediates, especially $p\mathrm{pR}_M$ and $p\mathrm{pR}_O$ states can be tailored by various techniques [25]–[29]. For instance, addition of azide affects the $p\mathrm{pR}_M$ state life time and replacing the amino acid (Val-108) by mathionine (Val-108 mutant of *p*pR) causes three times faster decay of $p\mathrm{pR}_M$ state and removes the shoulder of its spectrum [25]–[29].

Theoretical simulations for $p\mathrm{pR}_O$ state dynamics at a particular frequency (1.53 Hz) are shown in Fig. 9. At lower τ_O values, the population of initial *p*pR state is much greater than the population of the shorter lived $p\mathrm{pR}_O$ state. As modulating pulse appears, the TSI at 560 nm increases (positive switching) due to depletion of population of initial *p*pR state, which has a significant absorption at 560 nm, Fig. 9(a). An increase in τ_O results in peak TSI shifting towards the peak of modulating pulse with decrease in its contrast. This is due to decrease in contribution of

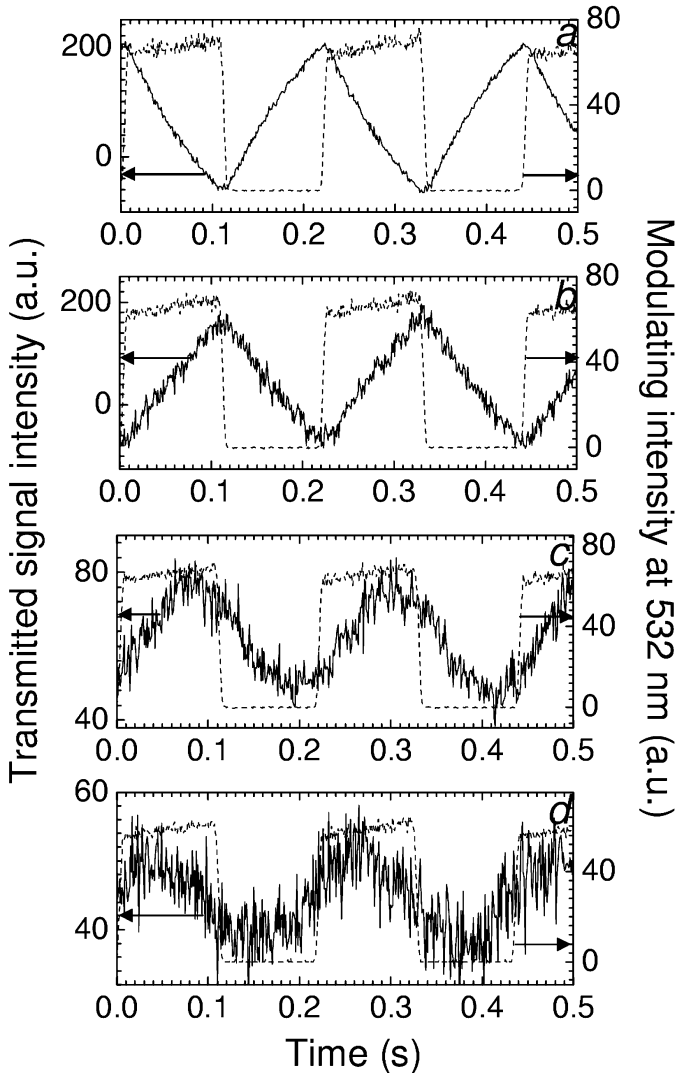

Fig. 7. Measured TSI at: (a) 390 nm; (b) 500 nm, (c) 560 nm; and (d) 600 nm (solid lines) and modulating beam at 532 nm (dashed lines) for modulating pulse frequency at 5 Hz.

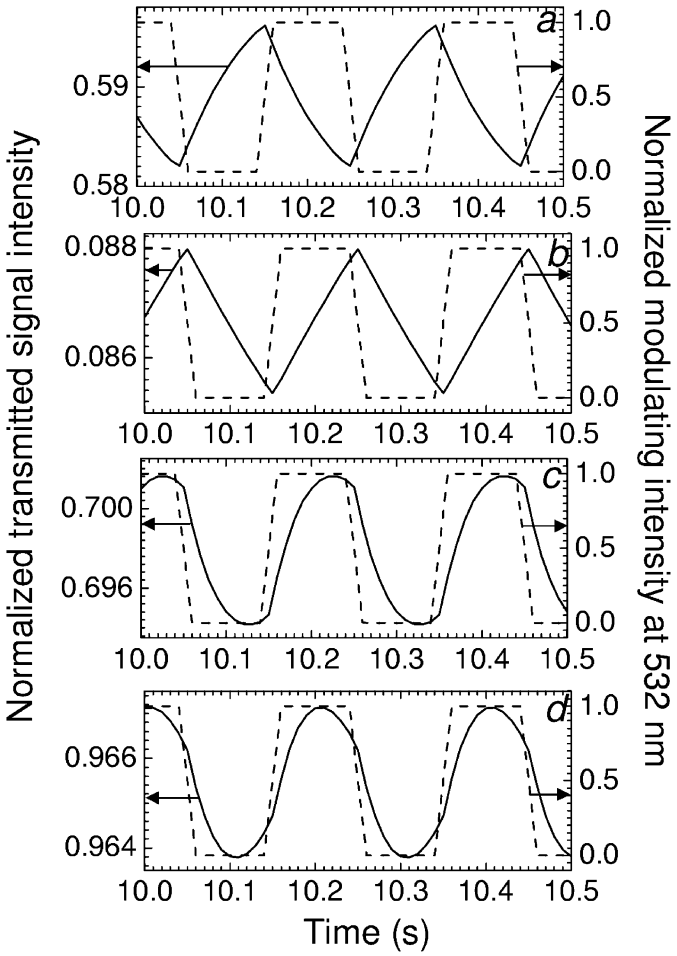

Fig. 8. Simulated normalized TSI at: (a) 390 nm; (b) 500 nm; (c) 560 nm; and (d) 600 nm (solid lines), and modulating beam at 532 nm (dashed lines) with modulating pulse frequency 5 Hz, for peak modulating power of 1 mW and signal beam power of 0.2 mW, respectively. Signal beam at 500 nm has been considered to be very weak.

ppR state to switching in comparison to $p\text{pR}_O$ state. At a particular τ_O value, the TSI becomes completely in-phase and also exhibits a super-gaussian-like profile. Further increase in τ_O shifts the peak of TSI towards increasing edge of modulating intensity. At particular τ_O value (15 ms), the TSI becomes out-of-phase with modulating intensity, due to increased absorption of signal beam at 560 nm by highly populated longer lived $p\text{pR}_O$ state, as discussed earlier, Fig. 5(a), (b). At higher τ_O values, the peak of TSI further shifts from increasing edge of modulating intensity towards its peak value, as shown in Fig. 9(b). The contrast of TSI decreases and then increases with increase in τ_O values. It is clear from Fig. 9 that the profile of TSI is also sensitive to the τ_O values.

Since the apparent phase shift in switching characteristics appears due to time taken by excited molecules to relax from the long lived $p\text{pR}_M$ state to the probed $p\text{pR}_O$ state, hence, for a fixed modulating frequency (f), increase in $p\text{pR}_M$ state lifetime (τ_M) would result in a similar variation as in Figs. 5 and 6, as shown in Fig. 10. An increase in τ_M from 0.001 s–0.7 s, keeping the frequency fixed at 1.53 Hz, results in an apparent phase shift of the peak of the switched signal beam from increasing to decreasing edges of the modulating pulses. Hence, a corresponding increase in τ_M at constant frequency results in a monotonic variation in apparent phase shift. The lifetime of $p\text{pR}'$ state appears to have no effect on the switching characteristics.

In general, the apparent phase shift appears when the modulating pulse width $(\sim 1/2f)$ becomes of the order of the rate constant of an earlier longer lifetime intermediate, in the range in which experiments have been conducted. The variation of apparent phase shift in this frequency range depends on the lifetimes of the probed excited state and its earlier intermediates. A theoretical fit of the experimental switching curves at different modulating frequencies would result in the estimation of the lifetimes of $p\text{pR}_M$ and $p\text{pR}_O$ states.

Fig. 11 shows the switching characteristics at different signal wavelengths at a higher value of $I'_{m0} = 500$ mW/cm^2. On comparison with Fig. 8, it is clear that the switching contrast increases with increase in I'_{m0}. Our simulations show that it saturates at higher values. Increase in I'_{m0} leads to the TSI at 390, 560, and 600 nm shifting towards lower values due to increase in the population of the respective probed excited states. The TSI at

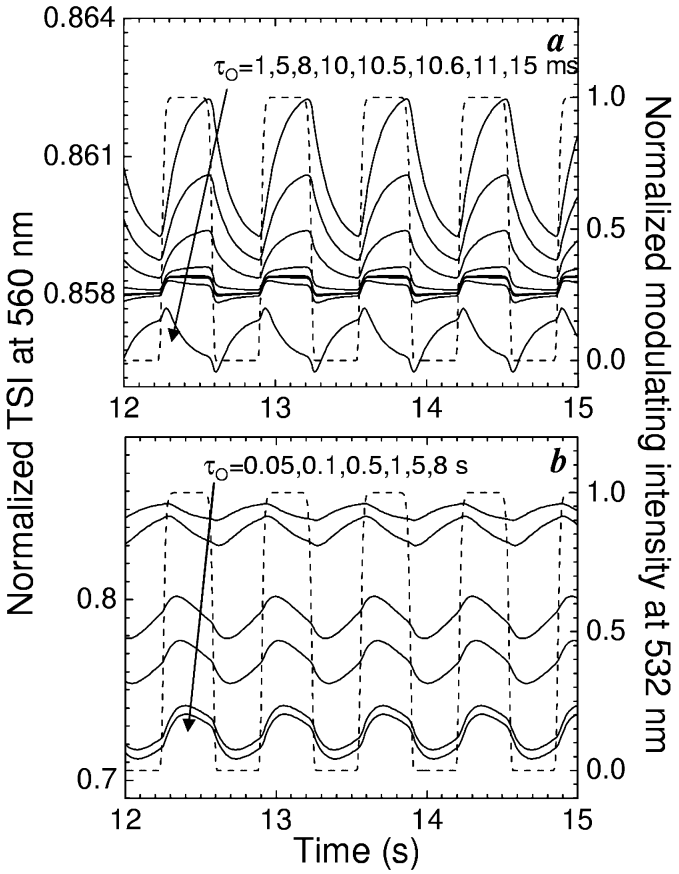

Fig. 9. Simulated normalized TSI at 560 nm (solid lines) for different τ_O values with $\tau_M = 112$ ms, and modulating beam at 532 nm (dashed lines) with modulating pulse frequency 1.53 Hz, for peak modulating power of 1 mW and signal beam power of 0.2 mW, respectively.

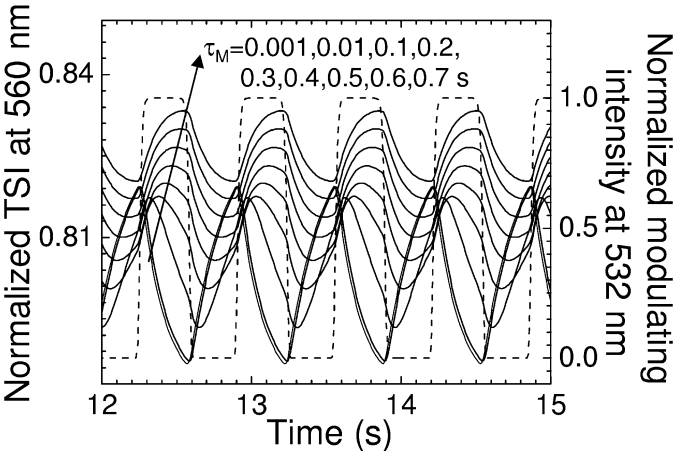

Fig. 10. Simulated normalized TSI at 560 nm (solid lines) for different τ_M values with $\tau_O = 323$ ms, and modulating beam at 532 nm (dashed lines) with modulating pulse frequency 1.53 Hz, for peak modulating power of 1 mW and signal beam power of 0.2 mW, respectively.

500 nm shifts towards higher values due to decrease in the population of the initial *p*pR state that gets depleted due to increased pumping by the modulating pulse at 532 nm. The switching contrast of TSI at 390, 500, 560 and 600 nm is 25.78%, 33.06%, 55.66% and 31.84%, respectively, as shown in Fig. 11. It can also be increased by using the modulating beam at 498 nm.

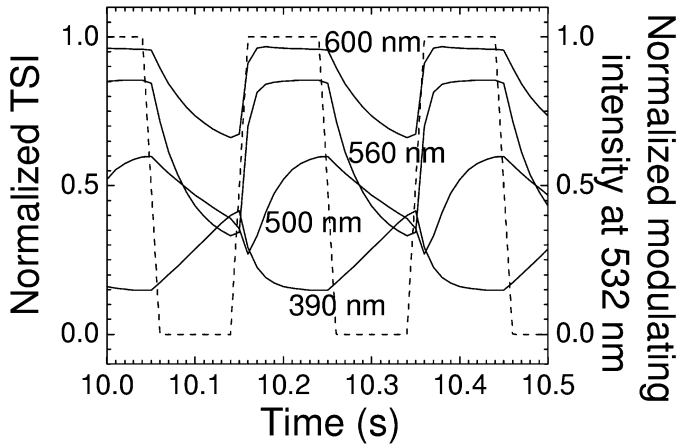

Fig. 11. Simulated normalized TSI at: (a) 390, (b) 500, (c) 560, and (d) 600 nm (solid lines), and modulating beam at 532 nm (dashed lines) with modulating pulse frequency 5 Hz, for peak modulating intensity of 500 mW/cm^2 and signal beam power of 0.2 mW, respectively. Signal beam at 500 nm has been considered to be very weak.

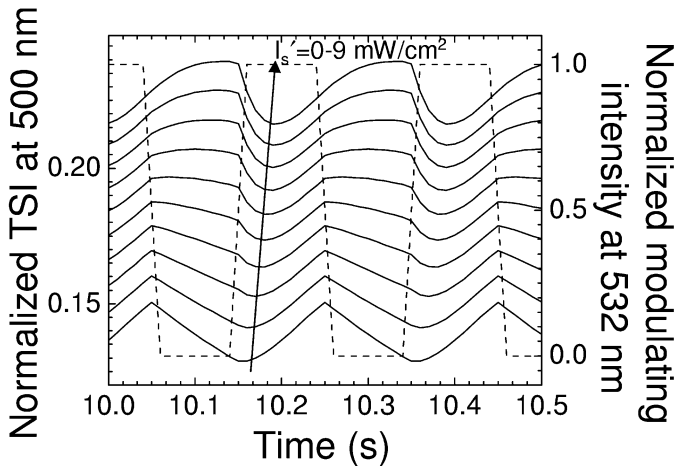

Fig. 12. Simulated normalized TSI at 500 nm (solid lines), and modulating beam at 532 nm (dashed lines) for modulating pulse frequency 1.53 Hz for peak modulating intensity of 50 mW/cm^2, for different signal beam intensity values.

The switching characteristics are also sensitive to signal intensity I'_s. Fig. 12 shows the variation in the switching characteristics with increase in I'_s. For a weak I'_s at 500 nm, the switching characteristics exhibit positive switching as shown in Figs. 7(b) and 8(b). The signal wavelength at 500 nm corresponds to the peak absorption of initial *p*pR state and the modulating wavelength at 532 nm is nearer to peak absorption wavelength of $p\text{pR}_O$ state [20], [21]. Hence, for increased values of I'_s, initially, in the absence of the modulating pulse, I'_s induces the photocycle by exciting the initial *p*pR state and leads to relatively higher TSI due to the depleted population of the *p*pR state. The appearance of the modulating pulse at 532 nm switches the $p\text{pR}_O$ state molecules back to initial *p*pR state. This results in increase in absorption of signal beam at 500 nm by increased population of the initial *p*pR state and leads to out-of-phase switching characteristics. Thus, for this case, the switching characteristics can be varied from in-phase to out-of-phase by considering the absorption by I'_m ($I'_{m0} = 50$ mW/cm^2) and varying I'_s from negligible values to 9 mW/cm^2, as shown in Fig. 12. The

variation in I'_s at 390, 560, and 600 nm in the same range has no effect on the apparent phase shift.

The apparent phase shift and profile of the TSI, which are sensitive to the kinetic and spectral response of the photointermediates, may possibly be useful to characterize *p*pR like proteins and to generate different forms of pulsed signal beams. Since the initial *p*pR state exhibits absorption over a broad visible range around 500 nm and the $p\text{pR}_M$ intermediate covers UV region around 390 nm and has a long lifetime, UV radiation can be blocked by *p*pR excited by visible light. The absorption spectra of different intermediates spanning the entire visible spectrum provide possibilities of nonlinear absorption at multiple wavelengths, which can be useful in the design of all-optical devices at different wavelengths.

Since *p*pR exhibits a blue-shifted photocycle with characteristics such as number of intermediates, overlap of absorption spectra of intermediates, and long lifetime intermediates in the later part of the photocycle similar to that of bR, the qualitative features of all-optical switching based on excited-state absorption are similar. The control of the apparent phase shift between the switched signal and the modulating beams and the profile of TSI currently studied in *p*pR would therefore also be observed in bR. The existence of longer lifetime states in the native WT form of *p*pR leads to switching at relatively lower modulating powers than bR, at the expense of slower switching time.

Since the kinetic and spectral properties of *p*pR can also be tailored by physical, chemical, and genetic engineering techniques, the switching characteristics can be optimized to increase the contrast and obtain faster response time [20]–[29]. Recently, new *p*pR mutants (T204C, T204S, S/E/T/A, S/E/T/C, S/E/T/S, etc.) with azide have been reported which exhibit the $p\text{pR}_M$ and $p\text{pR}_O$ state decays $\sim$ ms, respectively, which is comparable to that in bR [29]. Hence, *p*pR can provide switching time of the same order as bR. No photo degradation was observed even after performing a series of experiments at high I'_m values $(\sim 4\ \text{W/cm}^2)$ and continuous operation over a long time demonstrates the good thermal stability of *p*pR. Although in the experimental setup, the modulating and signal beams were arranged perpendicular to each other, they can be made to interact at small angles in practice, which would increase the interaction length and result in higher switching contrast.

The current study has been performed with *p*pR in liquid form. For practical applications, it would be more useful to have *p*pR films. So far, we have not tried to prepare *p*pR films. To the best of our knowledge, *p*pR films have also not been reported as yet. We are currently making efforts to prepare *p*pR films to enhance its utility for photonic applications.

V. Conclusion

All-optical switching in *p*pR protein has been studied based on nonlinear excited-state absorption. A modulating pulsed 532-nm laser beam has been shown to switch the transmission of a cw signal light beam at 390, 500, 560, and 600 nm, respectively. Simulations based on rate equation approach considering all seven states in the *p*pR photocycle are in good agreement with experimental results. The apparent phase shift of TSI with respect to modulating pulses and profile of the switched signal beam are sensitive to the frequency of the modulating pulses, and the signal beam intensity and wavelength. It is shown that the apparent phase shift of the switched signal beam at 560 and 600 nm, respectively, with respect to modulating pulsed beam can be varied to exhibit negative to positive switching. The switching characteristics at 500 nm can be inverted by increasing the signal beam intensity. The results show the applicability of *p*pR as a low-power wavelength tunable switch. The results also show the suitability of *p*pR as a new material for photonic applications in information processing such as switching, filtering, spatial light modulation, logic operations, etc., based on its photochromic properties.

Acknowledgment

The authors would like to thank Mr. T. Nishihori, Hokkaido University, Japan for preparing the *p*pR sample.

References

[1] K. Clays, "Molecular nonlinear optics: From para-nitroaniline to electrochemical switching of the hyperpolarizability," *J. Nonlinear Opt. Phys. Mater.*, vol. 12, pp. 475–495, 2003.

[2] F. M. Raymo, "Digital processing and communication with molecular switches," *Adv. Mater.*, vol. 14, pp. 401–414, 2002.

[3] D. Oesterhelt, C. Bräuchle, and N. Hampp, "Bacteriorhodopsin: a biological material for information processing," *Q. Rev. Biophys.*, vol. 24, pp. 425–478, 1991.

[4] R. R. Birge, "Protein based optical computing and memories," *Computer*, vol. 25, no. 11, pp. 56–67, Nov. 1992.

[5] M. H. Garzon and R. J. Deaton, "Biomolecular computing and programming," *IEEE Trans. Evol. Comput.*, vol. 3, no. 3, pp. 236–249, Sep. 1999.

[6] N. Hampp, "Bacteriorhodopsin as a photochromic retinal protein for optical memories," *Chem. Rev.*, vol. 100, pp. 1755–1776, 2000.

[7] J. A. Stuart, D. L. Marcy, K. J. Wise, and R. R. Birge, "Volumetric optical memory based on bacteriorhodopsin," *Synth. Met.*, vol. 127, pp. 3–15, 2002.

[8] A. L. Mikaelian and V. K. Salakhutdinov, "High-speed multichannel optical switching," *Proc. SPIE*, vol. 2144, pp. 84–90, 1994.

[9] S. Thai, J. Malowicki, and Q. Song, "Bacteriorhodopsin optical switch," *Proc. SPIE*, vol. 3384, pp. 107–118, 1998.

[10] P. Ormos, L. Fábián, L. Oroszi, E. K. Wolff, J. J. Ramsden, and A. Dér, "Protein based integrated optical switching and modulation," *Appl. Phys. Lett.*, vol. 80, pp. 4060–4062, 2002.

[11] P. Wu, D. V. G. L. N. Rao, B. R. Kimball, M. Nakashima, and B. S. DeCristofano, "Enhancement of photoinduced anisotropy and all-optical switching in bacteriorhodopsin films," *Appl. Phys. Lett.*, vol. 81, pp. 3888–3890, 2002.

[12] Y. Huang, S. T. Wu, and Y. Zhao, "Photonic switching based on the photoinduced birefringence in bacteriorhodopsin films," *Appl. Phys. Lett.*, vol. 84, pp. 2028–2030, 2004.

[13] C. P. Singh and S. Roy, "All-optical switching in bacteriorhodopsin based on M state dynamics and its application to photonic logic gates," *Opt. Commun.*, vol. 218, pp. 55–66, 2003.

[14] S. Roy, P. Sharma, A. K. Dharmadhikari, and D. Mathur, "All-optical switching with bacteriorhodopsin," *Opt. Commun.*, vol. 237, pp. 251–256, 2004.

[15] Y. Huang, S. T. Wu, and Y. Zhao, "All-optical switching characteristics in bacteriorhodopsin and its applications in integrated optics," *Opt. Express*, vol. 12, pp. 895–906, 2004.

[16] R. K. Banyal and B. R. Prasad, "High-contrast, all-optical switching in bacteriorhodopsin films," *Appl. Opt.*, vol. 44, pp. 5497–5503, 2005.

[17] J. L. Spudich and L. Hartmut, "Sensory rhodopsin II: Functional insights from structure," *Curr. Opin. Struct. Biol.*, vol. 12, pp. 540–546, 2002.

[18] R. Moukhametzianov, J. P. Klare, R. Efremov, C. Baeken, A. Göppner, J. Labahn, M. Engelhard, G. Büldt, and V. I. Gordelie, "Development of the signal in sensory rhodopsin and its transfer to the cognate transducer," *Nature*, vol. 440, pp. 115–119, 2006.

[19] N. Kamo, K. Shimono, M. Iwamoto, and Y. Sudo, "Photochemistry and photoinduced proton transfer by pharaonis phoborhodopsin," *Biochem.*, vol. 66, pp. 1277–1282, 2001.

[20] M. Miyazaki, J. Hirayama, M. Hayakawa, and N. Kamo, "Flash photolysis study on pharaonis phoborhodopsin from a haloalkaliphilic bacterium (Natronobacterium pharaonis)," *Biochim. Biophys. Acta*, vol. 1140, pp. 22–29, 1992.
[21] Y. Imamoto, Y. Shichida, J. Hirayama, H. Tomioka, N. Kamo, and T. Yoshizawa, "Nanosecond laser photolysis of phoborhodopsin: from natronobacterium pharaonis appearance of KL and L intermediates in the photocycle at room temperature," *Photochem. Photobiol.*, vol. 56, pp. 1129–1134, 1992.
[22] C. P. Singh, P. Sharma, and S. Roy, "Spatial light modulation with pharaonis phoborhodopsin," *IEE Proc. Circuits, Dev. Syst.*, vol. 150, pp. 563–568, 2003.
[23] P. Sharma and S. Roy, "All-optical light modulation in pharaonis phoborhodopsin and its application to parallel logic gates," *J. Appl. Phys.*, vol. 96, pp. 1687–1695, 2004.
[24] P. Sharma, S. Roy, and C. P. Singh, "Low power spatial light modulator with pharaonis phoborhodopsin," *Thin Solid Films*, vol. 477, pp. 227–232, 2005.
[25] M. Iwamoto, K. Shimono, M. Sumi, and N. Kamo, "Positioning proton-donating residues to the shiff-base accelerates the M-decay of pharaonis Phoborhodopsin expressed in Escherichia coli," *Biophys. Chem.*, vol. 79, pp. 187–192, 1999.
[26] K. Takao, T. Kikukawa, T. Araiso, and N. Kamo, "Azide accelerates the decay of M-intermediate of pharaonis Phoborhodopsin," *Biophys. Chem.*, vol. 73, pp. 145–153, 1998.
[27] Y. Sudo, M. Iwamoto, K. Shimono, and N. Kamo, "Association of pharaonis phoborhodopsin with its cognate transducer decreases the photo-dependent reactivity by water-soluble reagents of azide and hydroxylamine," *Biochim. Biophys. Acta*, vol. 1558, pp. 63–69, 2002.
[28] K. Shimono, M. Iwamoto, M. Sumi, and N. Kamo, "V108M mutant of pharaonis phoborhodopsin: substitution caused no absorption change but affected its M-state," *J. Biochem.*, vol. 124, pp. 404–409, 1998.
[29] M. Iwamoto, Y. Sudo, K. Shimono, T. Araiso, and N. Kamo, "Correlation of the O-intermediate rate with the pKa of Adp75 in the dark, the counterion of the Schiff base of pharaonis phoborhodopsin (sensory rhodopsins II)," *Biophys. J.*, vol. 88, pp. 1215–1223, 2005.

Sukhdev Roy received the B.Sc. (Hons.) degree in physics from Delhi University, Delhi, India, in 1986, the M.Sc. degree in physics with specialization in electronic science from Dayalbagh Educational Institute, Agra, India, in 1988, and the Ph.D. degree in physics from the Indian Institute of Technology, Delhi, in 1993.

From 1988 to 1989, he was a Senior Research Assistant in the Department of Physics, Indian Institute of Technology. Since 1993, he has been with the Department of Physics and Computer Science, Dayalbagh Educational Institute, where he is at present a Reader. In the summers of 2002–2004, he was also a Visiting Scientist at the Tata Institute of Fundamental Research, Mumbai, India. His areas of interest are nanophotonics and all-optical information processing.

Dr. Roy is a Member of the Optical Society of America, a Fellow of the Optical Society of India and a Life Member of the Indian Science Congress Association, Indian Laser Association, and the Biosensor Society, India. He was awarded the Best Paper Presentation Award by the Indian Science Congress Association in 2000 and 2001 and by the Systems Society of India in 1995. He was awarded the SERC Visiting Research Fellowship to the Department of Aerospace Engineering, Indian Institute of Science, Bangalore, in 1998; the Career Award for Young Teachers by the All-India Council for Technical Education, India, in 2001; and the Japan Society for Promotion of Science Invitation Fellowship to Hokkaido University, Sapporo, in 2004.

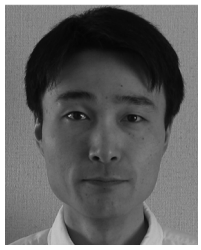

Takashi Kikukawa received the B.Eng. degree in electronic engineering and the M.Eng. and Ph.D. degrees in biomedical engineering from Hokkaido University, Sapporo, Japan, in 1991, 1993, and 1996, respectively.

From 1992 to 1996, he was with Research Institute for Electronic Science, Hokkaido University. He is currently an Instructor with the Creative Research Initiative "Sosei," Hokkaido University. His current research interests are molecular physiology and photobiology.

Dr. Kikukawa is a Member of the Biophysical Society and the Membrane Society, Japan.

Parag Sharma was born on December 22, 1980. He received the B.Sc. degree from M.J.P. Rohilkhand University, Bareilly, India, in 2000 and the M.Sc. degree in physics with specialization in computer science from Dayalbagh Educational Institute, Agra, India, in 2002. He is currently working toward the Ph.D. degree in the Department of Physics and Computer Science, Dayalbagh Educational Institute, in the area of biomolecular photonics.

Mr. Sharma is a Student Member of Optical Society of America and the Society for Photo-Optical Instrumentation Engineers, and a Life Member of Indian Science Congress Association, Optical Society of India, and the Indian Laser Association. Mr. Sharma was awarded the Junior and Senior Research Fellowship by the Council of Scientific and Industrial Research, Government of India, in 2002 and 2004, respectively. He was awarded the N. N. Saha Award by the Indian Biophysical Society in 2003, and the Young Scientist Award by the Indian Science Congress Association, and the DST Award for participation in the 18th Meeting of Nobel Laureates in Physics and Students in Lindau, Germany, in 2004.

Naoki Kamo received the B.Sc. degree in chemistry and the M.Sc degree in polymer science from Osaka University, Osaka, Japan, in 1968 and 1970, respectively, and the D.Sc degree in polymer science from Hokkaido University, Sapporo, Japan, in 1975.

From 1971 to 1979, he was a Research Assistant in the Faculty of Pharmaceutical Sciences of Hokkaido University. From 1979 to 1980, he was a Postdoctoral Fellow at the University of California, Berkeley. From 1980 to 1989, he was an Associate Professor in the Faculty of Pharmaceutical Sciences of Hokkaido University, and in 1989 he was promoted to full Professor. His research interest is in microbial rhodopsins containing bacteriorhodopsin, halorhodopsin, sensory rhodopsin, and phoborhodopsin, as well as membrane transport phenomena.

Prof. Kamo is a Member of the Biophysical Society (USA), Biophysical Society of Japan, Biochemical Society of Japan, and Pharmaceutical Society of Japan.